The Critical Role of the Underlayer Material and Thickness in Growing Vertically Aligned Carbon Nanotubes and Nanofibers on Metallic Substrates by Chemical Vapor Deposition

ARTICLE *in* ADVANCED FUNCTIONAL MATERIALS · APRIL 2010

Impact Factor: 11.81 · DOI: 10.1002/adfm.200902265

5 AUTHORS, INCLUDING:

Gilbert Daniel Nessim
Bar Ilan University
26 PUBLICATIONS **435** CITATIONS
SEE PROFILE

Matteo Seita
Massachusetts Institute of Technology
15 PUBLICATIONS **321** CITATIONS
SEE PROFILE

ADVANCED FUNCTIONAL MATERIALS
www.afm-journal.de

Materials Views
www.MaterialsViews.com

The Critical Role of the Underlayer Material and Thickness in Growing Vertically Aligned Carbon Nanotubes and Nanofibers on Metallic Substrates by Chemical Vapor Deposition

By *Gilbert D. Nessim, Donatello Acquaviva, Matteo Seita, Kevin P. O'Brien,* and *Carl V. Thompson**

Vertically aligned carbon nanotubes and nanofibers are grown on metallic Ta and Pd underlayers at temperatures below 500 °C. Controlling the size of the grains of the underlayer film is critical because this leads to a more uniform distribution of catalyst dots, which in turn results in vertical alignment of the carbon nanostructures. Rapid and limited heating and appropriate materials selection can also be used to limit catalyst/underlayer reactions that hinder or suppress carbon nanostructure growth or that lead to entangled growth. Control of catalyst reactivity with metallic underlayers is significant because growth on conductive substrates is notoriously difficult, but needed for many applications such as the use of carbon nanostructures in microelectronic circuits.

1. Introduction

Since their first characterization in 1991,[1] carbon nanotubes (CNTs) have been investigated for many applications given their exceptional electrical,[2] thermal,[3,4] and mechanical properties.[5,6] Applications such as replacing copper as the primary interconnect material for future integrated circuit technology require growth of vertically aligned CNTs on metallic underlayers at complementary metal–oxide–semiconductor (CMOS)-compatible temperatures (400–450 °C). CNT synthesis on metallic underlayers is especially difficult and most of the CNT synthesis literature focuses on the easier task of growing carpets of crystalline CNTs on electrically insulating (non-metallic) substrates such as alumina or silicon oxide using thermal chemical vapor deposition (CVD)[7–10] at temperatures between 700 and 900 °C. Although recent studies have shown encouraging progress toward growth on metallic substrates,[11,12] with some at growth temperatures approaching 400 °C (the requirement for CMOS compatibility),[13–16] few have focused on the critical role of the interactions between catalysts and metallic underlayers in limiting or enabling CNT growth. The focus of this work is to give an in-depth analysis of how the underlayer microstructure can affect the growth of CNT carpets.

Probably the most significant difference between CNT growth on insulating substrates compared to growth on conductive substrates when using the thermal CVD technique is the concurrent microstructure evolution of the metallic substrate and of the catalyst layer prior to CNT growth. Several phenomena including interdiffusion and alloying between catalyst and underlayer materials affect the dewetting process through which catalyst particles form.

There are few reports in the literature of relevant studies on the effects of metal underlayer material when growing CNTs by thermal CVD.[17–20] For instance, Lee et al.[18] investigated the effects of Cr, Ti, Ta, and W as the metal underlayers for CNT growth in a hot filament system with a sample temperature of 700 °C and using a Ni/Fe alloy as catalyst. The metal underlayers were nominally 100-nm thick with a grain size of roughly 20–30 nm in diameter and were sputter-deposited on silicon wafers. Lee et al. showed that the Ta and Ti underlayers were more suitable for CNT growth as, from the very beginning of the CVD process, the formation of silicide phases was favored over the formation of carbide phases, allowing the carbon feedstock to mainly interact with the catalyst metal to form nanotubes. In contrast, using Cr or W as an underlayer material resulted in the formation of a carbide and depletion of the available carbon, leading to insufficient carbon supply for the catalytic metals and therefore hindered nanotube growth. It should be noted that in both cases, the final substrate material was not metallic.

[*] Prof. C. V. Thompson, Dr. G. D. Nessim
Department of Materials Science and Engineering
Massachusetts Institute of Technology
77 Massachusetts Avenue, Cambridge, MA 02139 (USA)
E-mail: cthomp@mit.edu
D. Acquaviva
Laboratory of Micro and Nanoelectronics Devices
Ecole Polytechnique, Fédérale de Lausanne (EPFL), Bât ELB 339
Station 11, 1015 Lausanne (Switzerland)
M. Seita
Department of Materials, ETH Zürich
Wolfgang-Pauli-Str., CH-8093 Zürich (Switzerland)
Dr. K. P. O'Brien
Components Research department, Intel Corporation
Hillsboro, Oregon 97124 (USA)

DOI: 10.1002/adfm.200902265

Other studies showed that the thickness of the underlayer also affects and controls CNT growth. Delzeit et al.[17] observed that, using Fe as a catalyst, CNTs were obtained on 20-nm-thick Ir underlayers, but that no growth was achieved for Ir thicknesses of 5 or 40 nm. Considering that impurities such as oxygen can influence the kinetics of dewetting as Fillot et al.[21] showed for Cu on Ta substrates, we can infer that the dewetting, surface diffusion, and coarsening of a catalyst on the underlayer are likely to be affected by the underlayer thickness through effects on the surface composition. More recent work by Burt et al.[20] focused on the effect of the microstructure of aluminum underlayers on CNT growth. They studied the evolution of CNT carpets as a function of the Al underlayer deposition temperature and hence the film grain size. They then correlated the Al film microstructure with the carpet density and height, finding an optimum range of temperatures that led to CNT growth.

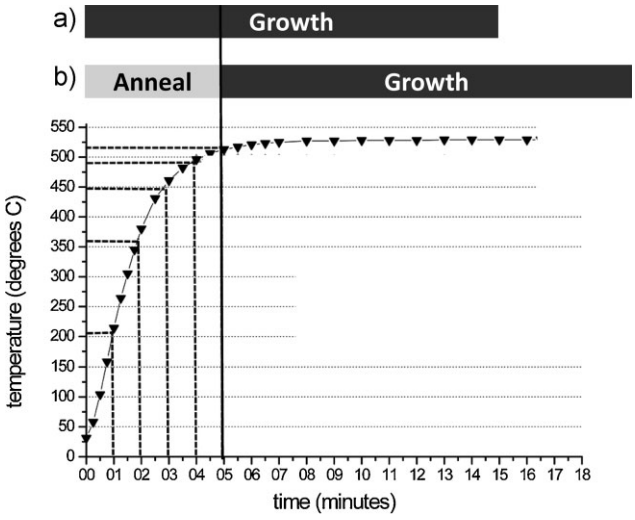

Figure 1. Temperature profile measured using a thermocouple positioned behind the sample showing that over 90% of the final temperature is reached within 5 min (at $t = 0$ the sample is introduced in the furnace using a ''fast-heat'' technique [14]). a) Schematic of a 15-min growth cycle without annealing. b) Schematic of a 5-min annealing cycle followed by 15 min of CNT growth.

2. Ni Catalysts on Pd Underlayers

2.1. Experiments

To investigate the influence of the microstructure of the metal underlayer on the growth of carbon nanotube/nanofiber carpets, we first compared growth on samples with 5 nm thick Ni catalyst layers on Pd layers of 25 and 500 nm thickness. As our goal was to grow CNTs on conductive layers for interconnect applications, Pd was chosen because it provides a reliable ohmic contact with CNTs.[22] Since the terminal grain size resulting from grain growth is limited to about three times the film thickness,[23,24] by using two different thicknesses of the metal underlayer, the underlayer grain size was varied without varying the growth conditions. We used a fast-heat technique in which we introduced the samples into the furnace only after the temperatures were stabilized.[14] The time dependence of the temperature measured using a thermocouple positioned behind the sample is shown in Figure 1. The final temperature was reached about 5 min after the sample was introduced into the furnace.

We performed two types of growth experiments, one in which all gases (Ar, H_2, and C_2H_4) were present at the moment we introduced the sample into the furnace (Fig. 1a), and another in which the substrate and catalyst were annealed in Ar/H_2 for increasing times (starting with the sample introduction into the furnace) before growth was initiated (H_2 annealing, Fig. 1b). For increasing H_2 annealing times (0, 2, and 5 min) followed by 15 min of growth, we observed vertical growth of carbon fibers on the samples with a thin Pd layer (upper scanning electron microscopy (SEM) images in Fig. 2a–c) compared to entangled growth (lower SEM images in Fig. 2a and b) or almost no growth (lower image in Fig. 2c) on the sample with a thick Pd layer. To observe the catalyst structure we did a shorter (5 min) growth and the corresponding SEM images indicated a higher density of fiber growth sites on the sample with a thin Pd layer compared to the sample with a thick Pd layer (Fig. 2d). We also carried out a short anneal (5 min) without growth (no ethylene introduced) and again observed a high density of dots (which we assumed to be Ni) on the sample with a thin Pd layer while only large Pd grains could be seen on the sample with a thick Pd layer. Backscattering at maximum contrast showed no Ni was present on the surface of the Pd grains (Fig. 2e). The carbon structures grown in the experiment illustrated in Figure 2a were characterized using high-resolution transmission electron microscopy (HRTEM) and were found to be nanofibers (not shown), from which we inferred that all the structures shown in Figure 2 were most likely noncrystalline fibers. Figure 2 clearly showed a strong difference between the fiber growth obtained on the thin and the thick Pd films, suggesting that fiber coverage and nucleation depend on the underlayer grain size. Given the entangled nanofiber formation on samples with a thick Pd underlayer, we hypothesize that, upon annealing, the nickel migrated and decorated the grain boundaries of the thick Pd films so that the density of carbon fibers was low and the lack of steric hindrance led to entangled growth.[25] In the case of the thin, small-grained Pd film, the catalysts and carbon fibers were close enough for dense vertical growth. An additional experiment done on another sample with intermediate Pd layer thickness (200 nm) and using a short 5 min growth at 720 °C with a thermal ramp (compared to the ''fast-heat'' used in all the other experiments) showed distinct decoration of the Pd grain boundaries with Ni catalyst (Fig. 3).

2.2. Discussion

Ni and Pd form a solid solution for all compositions, there is no stable Ni–Pd intermetallic compound,[26] and the surface energy of Ni (calculated average value 1389 ergs cm^{-2}) is usually 10% to 30% higher compared to Pd (calculated average value 1097 ergs cm^{-2}), depending on the crystallographic orientation.[27,28] Although the evolution of the instability of a nanometer-thick film during dewetting is complex,[29] we will focus on specific aspects and hypothesize that Ni diffuses mainly

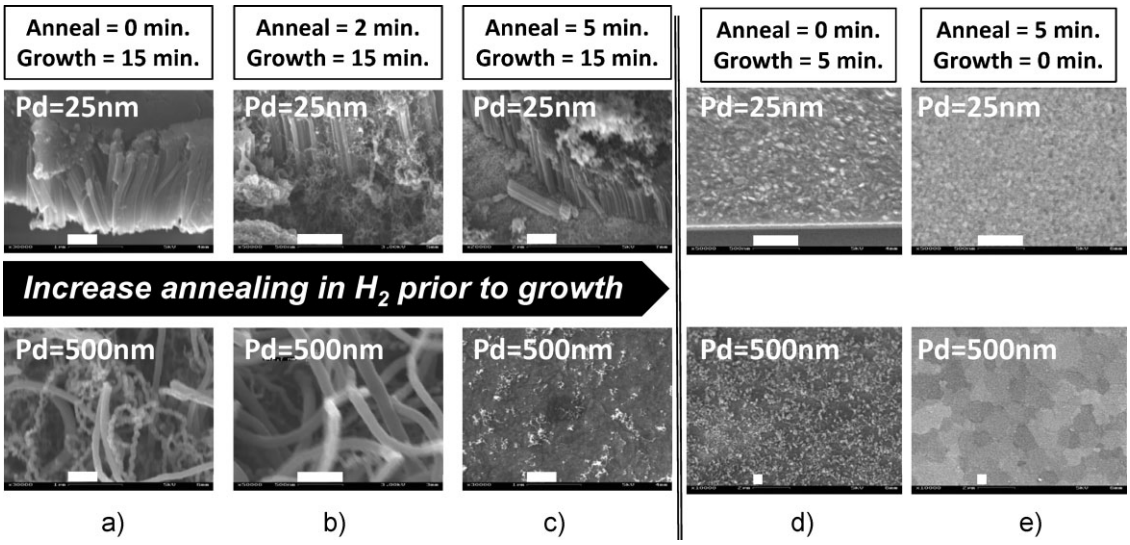

Figure 2. a–c) Comparison of results with a thin Pd layer (top, 25 nm) showing vertically aligned fiber growth and a thick Pd layer (bottom, 500 nm) showing entangled fiber growth (a,b) or almost no growth (c). d) Comparison of a short growth cycle for the sample with a thin Pd layer (top) showing a higher density of fibers compared to the sample with a thick Pd layer (bottom) showing more sparse fibers. e) Short anneal cycles (with no growth) showing dense dots on the sample with a thin Pd layer (top) while Pd grains and no dots were observed on the sample with a thick Pd layer (bottom). All samples were processed at a gas preheat temperature of 780 °C and a substrate temperature of 500 °C. The flow rates of $Ar/H_2/C_2H_4$ were 400/800/250 sccm. The scale bar on the SEM images is 500 nm.

by surface diffusion and that dewetting and particle formation is catalyzed at the grain boundaries, with the surfaces of the grains depleted of Ni so that no particles form there. As a consequence, the Pd boundaries are decorated by Ni particles at the end of the thermal treatment, which started with the sample being introduced into the furnace (fast heat) and ended when the sample was removed from the furnace. This hypothesis is consistent with the results reported by Hermann et al.[30] on the Ni–Al system in which Ni particles were predominantly positioned at the grain boundaries of the underlying Al film (100 nm thick) after a thermal annealing process at 500 °C in forming gas.

We estimated the values for the diffusivity of Ni in and on Pd using the formulas[31–34] given in Reference [35], which are valid for fcc metals:

$$D_L = 0.5 \exp(-17 \times T_M/T) \quad \text{in cm}^2\ \text{s}^{-1} \tag{1}$$

$$\delta D_{GB} = 1.5 \cdot 10^{-8} \exp(-8.9 \times T_M/T) \quad \text{in cm}^2\ \text{s}^{-1} \tag{2}$$

$$D_S = 0.014 \exp(-6.54 T_M/T) \quad \text{in cm}^2\ \text{s}^{-1} \tag{3}$$

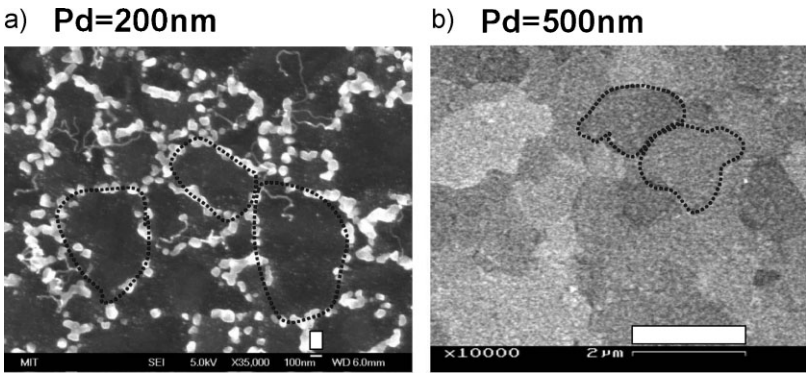

Figure 3. SEM images showing post-heat-treatment grain sizes in Pd films with two different thicknesses. Grain growth stagnates when the in-plane grain size is about three times the film thickness. a) Ni-decorating Pd grains of a sample with a 200-nm-thick Pd underlayer (processing: thermal ramp and 5-min growth at 720 °C). Short carbon nanofibers growing from a few catalysts can also be observed. Scale bar is 100 nm. b) Pd grains can be seen after a 5-min anneal ("fast-heat" in Ar/H_2) for a sample with a Pd layer of 500 nm thickness. Scale bar is 2 μm. This image is an enlargement of the lower SEM image shown in Figure 2e.

where D_L is the lattice diffusivity, T_M is the melting temperature of Pd (1825 K), δ is the grain boundary width (taken to be 0.5 nm), D_{GB} is the grain boundary diffusivity, and D_S is the surface diffusivity. We estimated the diffusion lengths by integrating the $\sqrt{4Dt}$ terms over time, with temperature being a function of time t (estimated using 25 °C intervals, with $t = 0$ when the sample is introduced into the furnace) and found values of $D_L \approx 0.3$ nm, $D_{GB} \approx 4.8\ \mu$m, and $D_S \approx 19\ \mu$m after 5 min. The "fast-heat" temperature profile is shown in Figure 1; the tables showing the calculation of the diffusion lengths can be found in the Supporting Information.

Ni and Pd should eventually mix to form a solid solution. However, our calculations indicate that, at our highest process temperature and after the first 5 min of processing, the total diffusion distance of Ni into Pd equals

only 0.3 nm. Even for 15 min of processing (the growth duration of most experiments) at 500 °C, the cumulative diffusion length would only be 0.8 nm, so that lattice diffusion is not a significant factor (especially for Ni depletion on the sample with a thick Pd layer for a 5-min annealing process).

We expected grain boundary diffusion to play a critical role, especially during the first few minutes of the processing, given that a 5-min anneal of the sample with a thick Pd layer almost did not exhibit nanofiber growth. Diffusion length calculations show that, considering grain boundary diffusion, after 3 min during our thermal process the cumulative grain boundary diffusion length would reach 500 nm, thus equaling the thickness of our thick Pd layer. Interestingly, the 3-min mark fits with the growth results obtained for the sample with a thick Pd layer where we observed entangled growth after a 2-min anneal but almost no growth after a 5-min anneal. This seems to suggest that, given enough time, the Ni would completely diffuse into the Pd grain boundaries at our process temperature. Moreover, calculations show that the cumulative surface diffusion length after 3 min (~3 μm) is larger than the estimated terminal grain size of the Pd film (~1.5 μm), which is consistent with our assumption that Ni particles would tend to segregate at the Pd grain boundaries. We first modeled the diffusion by considering fixed geometrical dimensions of our Ni and Pd grains, and of the grain boundary volume into which Ni can diffuse. We assumed that the Pd film is an ensemble of square grains of size $d = 75$ nm for the sample with a thin Pd layer (25 nm) and $d = 1500$ nm for the sample with a thick Pd layer (500 nm) in accordance with the terminal grain growth assumption that grains grow up to three times the film thickness.[23,24] Each grain was separated from its neighboring grains by a grain boundary of thickness δ, which was assumed to be 0.5 nm, and the thickness of the grain h equaled the thickness of the film. A pictorial representation (adapted from Ohring[35]) is shown in Figure 3.

Given that surface diffusion is at least one order of magnitude faster than grain boundary diffusion (at our highest temperature), we assumed that when the Ni film dewets, particles first form at the grain boundaries and then dissolve by diffusion into the grain boundaries, given sufficient time and temperature. Using our simplified film geometry, the flux of Ni into grain boundaries J_{GB} is 4×10^7 times compared to the flux of Ni into the lattice J_L ($J_{GB}/J_L = (h\ D_{GB})/(d\ D_L)$, assuming $d = 3h$). Considering our very small lattice diffusion lengths with respect to our Pd film thicknesses and that our D_{GB} is nine orders of magnitude higher than D_L, even at our highest process temperature, diffusion along the grain boundaries will dominate the kinetics of diffusion, which is what Harrison defines as the "type-C" regime of diffusion.[36]

We calculated the total grain boundary volume available for Ni to diffuse into both Pd film thicknesses (~3.3×10^{13} nm^3 for a 1 cm^2 sample) and found that it is 15 times smaller than the volume of the 5 nm thick Ni layer (~5×10^{14} nm^3 for a 1 cm^2 sample). From this we infer that grain boundary diffusion consumes only a small fraction of the nickel, leaving most of the Ni on the surface (likely as particles at the grain boundaries as observed with SEM in Fig. 2 and 3). The experimental results support this conclusion for the sample with a thin Pd layer for all our experiments, as we can still grow fiber carpets irrespective of the duration of the annealing and growth steps. However, this model is not supported by the results observed for the sample with a thick Pd layer after long anneals because after a 5-min anneal we did not observe fibers or Ni catalyst particles on the surface.

To explain the phenomenon observed for long annealing times of the sample with a thick Pd layer, we will consider the grain size evolution during the annealing process. The as-deposited grain structure for Pd should be constituted of non-equiaxed columnar grains with in-plane sizes that are significantly smaller than the film thickness.[37] Given that grain growth is not likely during the film deposition, we expect the in-plane grain size to be small and of comparable size for both Pd thicknesses (Fig. 4). Therefore, the terminal grain size of three times the film thickness requires grain growth during the anneal, with the total change in grain size, and consequently the volume through which grain boundaries sweep, being larger in the thicker film. If we assume that diffusion of the Ni into the grain boundaries occurs during grain growth, and that Ni is incorporated into the Pd lattice as grain boundaries sweep through the volume of the film, it would be reasonable to expect that more Ni is incorporated in the Pd lattice in the case of the thicker film, so that less Ni is left to form precipitates at the grain boundaries once grain growth stops (Fig. 5). This mechanism of incorporation of Ni into the Pd lattice is similar to the diffusion-induced grain boundary migration phenomenon.[38–41] This model is consistent with the experimental results obtained here for the thin Pd films where we always observed fiber growth, and for the thick Pd films where we observed fiber growth only when there was no annealing or when the annealing time did not exceed a few minutes.

3. Fe Catalysts on Ta Underlayers

To test the hypotheses drawn from the analysis of the Ni–Pd system, we compared growth on samples with a 5 nm thick Fe catalyst on Ta underlayers with thicknesses of 30 and 250 nm. Choosing a high-melting-point material such as tantalum (3290 K), we expected to decouple the effect of thermally induced grain growth from the diffusion of the catalyst material into the

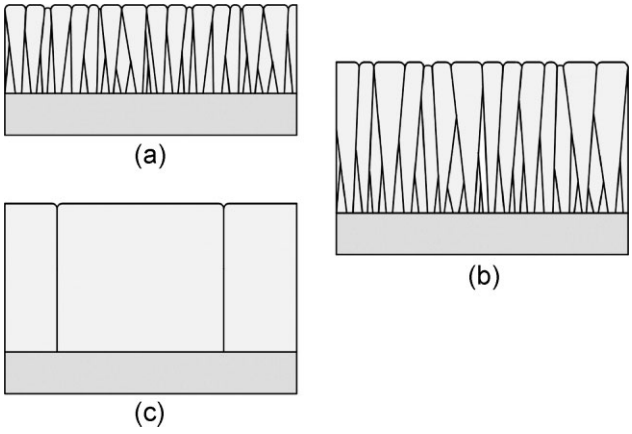

Figure 4. a) Structure of non-equiaxed columnar grains in an as-deposited thin film. b) Structure of non-equiaxed columnar grains of a thicker film as deposited; the in-plane grain sizes are comparable. c) Evolution of grain structure of thick film after grain growth (thermal treatment) showing a significant increase in the in-plane grain size. Drawings adapted from Reference [37].

underlayer grain boundaries. In earlier work we gained experience in growing dense carpets of crystalline vertically aligned carbon nanotubes using Fe as a catalyst with a 30 nm thick Ta underlayers.[14,42] In the current and earlier experiments we used a substrate temperature of 500 °C with a gas preheat temperature of 770 °C. Considering that the substrate temperature was around 500 °C, which corresponds to a homologous temperature of only 0.23 = 773 K/3290 K, we do not expect grain growth in the Ta during thermal processing leading to CNT growth.[37] However, given the non-equiaxed columnar structure of the Ta grains and grain occlusion during film thickening, we might expect the grain size at the surface of thicker films to be somewhat larger than at the surface of thinner films. However, for both film thicknesses, the grain size at the surface of the film should not change and should be significantly smaller than the film thickness.

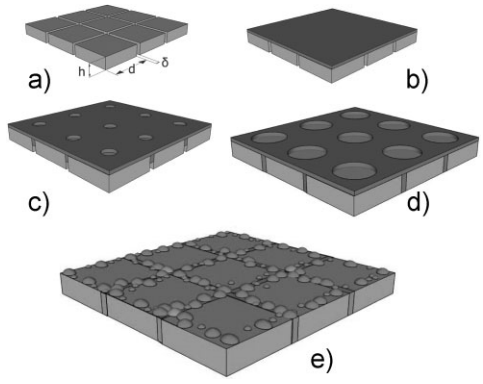

Figure 5. a) Idealized grain structure of a thin film for which each grain has a square shape of size *d*, thickness *h*, and is separated from the other grains by grain boundaries of thickness δ. b) Ni catalyst thin film deposited above the Pd underlayer. c) Ni thin film starts dewetting, moving to Pd grain boundaries, and diffusing into Pd grain boundaries. Pd grains start growing due to the thermal process. d) Further Ni dewetting, with Pd grains expanding and Ni alloying with swept Pd volume and further diffusing into Pd grain boundaries. e) Ni has saturated the grain boundaries and Pd grains have reached terminal size, thus leaving Ni dots on the surface decorating the Pd grain.

When we compared the carpets obtained after CNT synthesis for both Ta samples, we observed that the sample with a thicker Ta layer exhibited a marginally lower carpet density and slightly larger CNT diameters (Fig. 6). Given the lack of significant grain growth in Ta underlayers, this result is consistent with the hypotheses that smaller underlayer grains are an enabler of vertically aligned CNT growth. Even for Ta films sputtered and annealed at 800 °C, we still observed Ta grain sizes below 100 nm (Fig. 7), which demonstrates that grain growth would not occur in films annealed at lower temperatures.

4. Conclusions

In conclusion, we have analyzed the critical role of material and thickness of underlayers in carbon fiber and CNT growth by comparing samples with thin and thick underlayers for two

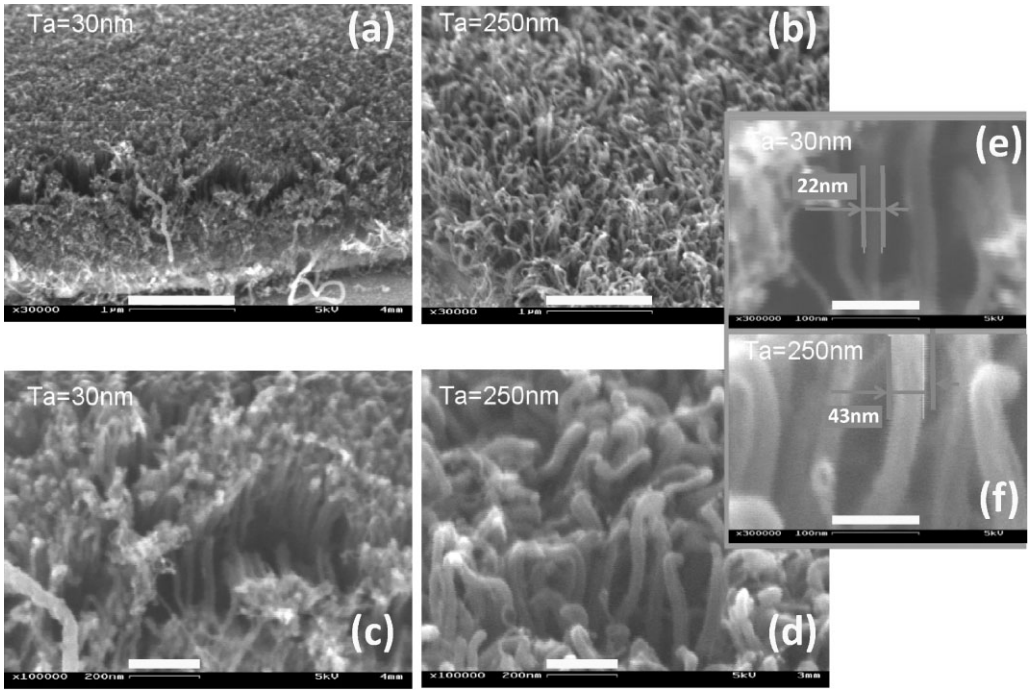

Figure 6. Comparison of growth for Fe–Ta samples with a thin 30-nm Ta layer (SEM images a, c, and e are different magnifications of the same sample) and samples with a thick 250-nm Ta layer (SEM images b, d, and f are different magnifications of the same sample). A slightly denser CNT carpet can be observed on the sample with a thin Ta layer (images a and c) compared to the sample with a thicker Ta layer (images b and d). The insets on the right show that CNTs grown on the sample with a thin Ta layer (image e) have a thinner diameter compared to the CNTs grown on the sample with a thicker Ta layer (image f). Process details: $Ar/H_2/C_2H_4 = 400/800/250$ sccm; $T = 780/780/475$ °C; 15 min growth (no anneal). Scale bars are 1 μm on images (a) and (b), 200 nm on images (c) and (d), and 100 nm on images (e) and (f).

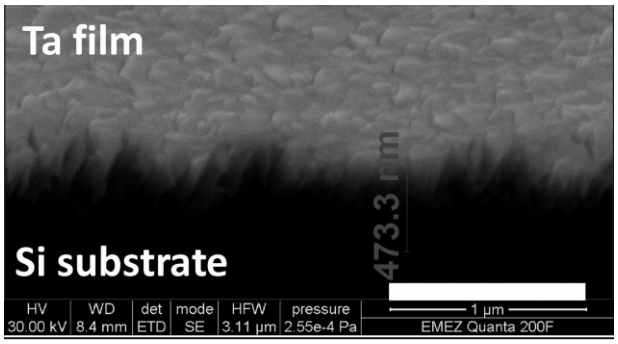

Figure 7. Cross section of a sample with a thick Ta layer (500 nm) sputtered on a silicon substrate heated at 800 °C. The average Ta grain size is still below 100 nm in size. Scale bar is 1 μm.

materials systems. An extensive series of anneal and growth experiments of increasing duration on a Ni–Pd catalyst-underlayer system showed that dense and aligned fiber growth was obtained for samples with a thin Pd underlayer (25 nm), while sparse and entangled growth or almost no growth was obtained on the samples with a thick underlayer (500 nm), under the same process conditions. By considering the characteristics of the grain structure and the kinetics of dewetting, diffusion, and grain evolution, we formulated a mechanism that is consistent with our experimental results, based on concomitant diffusion of Ni into Pd grain boundaries, grain growth in the Pd, and precipitation of the Ni left on the surface at Pd grain boundaries. Using Ta as the underlayer, a material with a higher melting temperature and lower grain boundary mobility compared to Pd, we were able to grow vertically aligned carpets of CNTs for thin (30 nm) and thick (250 nm) Ta layers, because the thermal process minimally affected the Ta grain size. However, we noted a slight decrease in the CNT density for the samples with a thick Ta layer, in accordance with a marginally larger grain size at the surface of the thicker film. Understanding the coupled influences of film thickness, grain size, and catalyst dewetting is an important step in development of a more complete understanding of CNT growth mechanisms, especially on metallic underlayers.

5. Experimental

All the samples used in this study were prepared using electron-beam evaporation of metallic thin films using a CHA bell jar evaporator with a four-pocket Temescal source at Intel. The base pressure was between 2.0×10^{-6} and 2.0×10^{-7} Torr. The samples were prepared on oxidized silicon substrates and were manually cleaved to form approximately 5 mm × 5 mm pieces that were used during the CNT growth experiments. Samples were cleaned with acetone and isopropyl alcohol prior to CNT growth. The Ni–Pd catalyst-underlayer samples had a blanket deposited Ta adhesion-promoting underlayer (5 nm thick), a Pd deposition underlayer (25 or 500 nm thick), and a Ni catalyst layer (5 nm thick). The Fe–Ta samples had a Ta deposition underlayer (30 or 250 nm thick) and an Fe catalyst layer (5 nm thick).

Growth was performed at atmospheric pressure using a three-zone furnace (Lindberg Blue) in a fused-silica tube with an internal diameter of 22 mm. Flows of Ar (99.9995%, Airgas), C_2H_4 (99.5%, Airgas), and H_2 (99.999%, Airgas) were maintained using electronic mass flow controllers (MKS 1179A). The samples were positioned in the quartz tube using a custom-made quartz fixture (Finkenbeiner Glass, Waltham, MA), and faced the flow at an inclination of 20°.

All experiments were performed using a "fast-heat" technique, in which the samples were initially positioned in the quartz tube outside the furnace with a fan blowing from below to keep the exposed quartz tube walls at room temperature (the technique is fully detailed and illustrated in Reference [14]). An argon flow was maintained while the three zones of the furnace were ramped to the desired temperature. Once the set temperatures were reached, hydrogen and ethylene were also introduced and the quartz tube was shifted (the sample is sitting on the fixture inside the quartz tube), thus positioning the sample in the growth zone and starting the CNT growth. After the growth was completed, the quartz tube was shifted out of the furnace to slowly cool down to room temperature under a flow of argon before removing the sample.

The preheat and the growth temperatures are indicated by the built-in furnace thermocouples. An additional thermocouple (Omega TJ36, accuracy 0.2 °C) connected to a digital temperature reader (Barnant 115) was inserted in the quartz tube (aligned with its axis) and positioned just behind the custom-made quartz fixture containing the sample. The CNTs were examined using high-resolution SEM (Zeiss/Leo Gemini 982, Philips XL30, and FEI Quanta 200 FEG with backscattering) and HRTEM (FEI Tecnai F30 FEG and Philips CM 30).

Acknowledgements

We thank Dr. Reiner Mönig, Dr. Amanda Giermann, Andrew Takahashi, and Robert Mitchell for useful discussions. We are grateful to the staff of the NanoStructures Laboratory (NSL) at MIT where we took our SEM images. This research was supported by the MARCO Interconnect Focus Center and the Singapore–MIT Alliance. G.D.N. was partially supported by an Intel Fellowship. Supporting Information is available online from Wiley InterScience or from the author.

Received: November 30, 2009
Revised: January 7, 2010
Published online: March 31, 2010

[1] S. Iijima, *Nature* **1991**, *354*, 56.
[2] J. Bernholc, D. Brenner, M. B. Nardelli, V. Meunier, C. Roland, *Annu. Rev. Mater. Res.* **2002**, *32*, 347.
[3] S. Berber, Y.-K. Kwon, D. Tománek, *Phys. Rev. Lett.* **2000**, *84*, 4613.
[4] T. Tong, Y. Zhao, L. Delzeit, A. Kashani, M. Meyyappan, A. Majumdar, *IEEE Trans. Compon. Packag. Technol.* **2007**, *30*, 92.
[5] R. H. Baughman, A. A. Zakhidov, W. A. de Heer, *Science* **2002**, *297*, 787.
[6] J. N. Coleman, U. Khan, W. J. Blau, Y. K. Gun'ko, *Carbon* **2006**, *44*, 1624.
[7] A. J. Hart, A. H. Slocum, *J. Phys. Chem. B* **2006**, *110*, 8250.
[8] K. Hata, D. N. Futaba, K. Mizuno, T. Namai, M. Yumura, S. Iijima, *Science* **2004**, *306*, 1362.
[9] T. Yamada, T. Namai, K. Hata, D. N. Futaba, K. Mizuno, J. Fan, M. Yudasaka, M. Yumura, S. Iijima, *Nat. Nanotechnol.* **2006**, *1*, 131.
[10] G. D. Nessim, A. J. Hart, J. S. Kim, D. Acquaviva, J. H. Oh, C. D. Morgan, M. Seita, J. S. Leib, C. V. Thompson, *Nano Lett.* **2008**, *8*, 3587.
[11] T. de los Arcos, F. Vonau, M. G. Garnier, V. Thommen, H. G. Boyen, P. Oelhafen, M. Duggelin, D. Mathis, R. Guggenheim, *Appl. Phys. Lett.* **2002**, *80*, 2383.
[12] Y. Y. Wang, Z. Q. Luo, B. Li, P. S. Ho, Z. Yao, L. Shi, E. N. Bryan, R. J. Nemanich, *J. Appl. Phys.* **2007**, *101*, 124310.
[13] Y. Awano, S. Sato, D. Kondo, M. Ohfuti, A. Kawabata, M. Nihei, N. Yokoyama, *Phys. Status Solidi A* **2006**, *203*, 3611.
[14] G. D. Nessim, M. Seita, K. P. O'Brien, A. J. Hart, R. K. Bonaparte, R. R. Mitchell, C. V. Thompson, *Nano Lett.* **2009**, *9*, 3398.
[15] M. Nihei, A. Kawabata, D. Kondo, M. Horibe, S. Sato, Y. Awano, *Jpn. J. Appl. Phys.* **2005**, *44*, 1626.
[16] D. Yokoyama, T. Iwasaki, K. Ishimaru, S. Sato, T. Hyakushima, M. Nihei, Y. Awano, H. Kawarada, *Jpn. J. Appl. Phys.* **2008**, *47*, 1985.

[17] L. Delzeit, B. Chen, A. Cassell, R. Stevens, C. Nguyen, M. Meyyappan, *Chem. Phys. Lett.* **2001**, *348*, 368.
[18] K. M. Lee, H. J. Han, S. H. Choi, K. H. Park, S. Oh, S. Lee, K. H. Koh, *J. Vacuum Sci. Technol. B* **2003**, *21*, 623.
[19] H. T. Ng, B. Chen, J. E. Koehne, A. M. Cassell, J. Li, J. Han, M. Meyyappan, *J. Phys. Chem. B* **2003**, *107*, 8484.
[20] D. P. Burt, W. M. Whyte, J. M. R. Weaver, A. Glidle, J. P. Edgeworth, J. V. Macpherson, P. S. Dobson, *J. Phys. Chem. C* **2009**, *113*, 15133.
[21] F. Fillot, Z. Tokei, G. P. Beyer, *Surf. Sci.* **2007**, *601*, 986.
[22] D. Mann, A. Javey, J. Kong, Q. Wang, H. J. Dai, *Nano Lett.* **2003**, *3*, 1541.
[23] H. J. Frost, C. V. Thompson, D. T. Walton, *Acta Metall. Mater.* **1990**, *38*, 1455.
[24] J. E. Palmer, C. V. Thompson, H. I. Smith, *J. Appl. Phys.* **1987**, *62*, 2492.
[25] C. J. Lee, D. W. Kim, T. J. Lee, Y. C. Choi, Y. S. Park, Y. H. Lee, W. B. Choi, N. S. Lee, G. S. Park, J. M. Kim, *Chem. Phys. Lett.* **1999**, *312*, 461.
[26] G. Ghosh, C. Kantner, G. B. Olson, *J. Phase Equilib.* **1999**, *20*, 295.
[27] Y. N. Wen, H. M. Zhang, *Solid State Commun.* **2007**, *144*, 163.
[28] J. M. Zhang, F. Ma, K. W. Xu, *Appl. Surf. Sci.* **2004**, *229*, 34.
[29] J. Becker, G. Grun, R. Seemann, H. Mantz, K. Jacobs, K. R. Mecke, R. Blossey, *Nat. Mater.* **2003**, *2*, 59.
[30] S. Hermann, R. Ecke, S. Schulz, T. Gessner, *Microelectron. Eng.* **2008**, *85*, 1979.
[31] D. Gupta, *Diffusion Processes in Advanced Technological Materials*, William Andrew Pub., Norwich, NY **2005**.
[32] D. Gupta, P. S. Ho, *Diffusion Phenomena in Thin Films and Microelectronic Materials*, Noyes Publications, Park Ridge, NJ **1988**.
[33] K. N. Tu, J. W. Mayer, L. C. Feldman, *Electronic Thin Film Science for Electrical Engineers and Materials Scientists*, Macmillan, New York **1992**.
[34] R. W. Balluffi, J. M. Blakely, *Thin Solid Films* **1975**, *25*, 363.
[35] M. Ohring, *The Materials Science of Thin Films: Deposition and Structure*, Academic Press, San Diego, CA **2002**.
[36] L. G. Harrison, *Trans. Faraday Soc.* **1961**, *57*, 1191.
[37] C. V. Thompson, *Annu. Rev. Mater. Sci.* **2000**, *30*, 159.
[38] M. Hillert, *Scr. Metall.* **1983**, *17*, 273.
[39] M. Hillert, G. R. Purdy, *Acta Metall.* **1978**, *26*, 333.
[40] J. D. Pan, R. W. Balluffi, *Acta Metall.* **1982**, *30*, 861.
[41] W.-H. Rhee, Y.-D. Song, D. N. Yoon, *Acta Metall.* **1987**, *35*, 57.
[42] G. D. Nessim, J. Oh, D. Acquaviva, M. Seita, N. Abate, H. Tang, K. P. O'Brien, C. V. Thompson, presented at *Materials Research Society, MRS Fall 2007 Conference, Symposium M*, Boston, MA, November 28, 2007.